

Influence of interfacial dislocations on hysteresis loops of ferroelectric films

Y. L. Li, S. Y. Hu, S. Choudhury, M. I. Baskes, A. Saxena, T. Lookman, Q. X. Jia, D. G. Schlom, and L. Q. Chen

Citation: [Journal of Applied Physics](#) **104**, 104110 (2008); doi: 10.1063/1.3021354

View online: <http://dx.doi.org/10.1063/1.3021354>

View Table of Contents: <http://scitation.aip.org/content/aip/journal/jap/104/10?ver=pdfcov>

Published by the [AIP Publishing](#)

Articles you may be interested in

[Nanosecond-range imprint and retention characterized from polarization-voltage hysteresis loops in insulating or leaky ferroelectric thin films](#)

Appl. Phys. Lett. **99**, 142905 (2011); 10.1063/1.3647577

[Depolarizing field and “real” hysteresis loops in nanometer-scale ferroelectric films](#)

Appl. Phys. Lett. **89**, 253108 (2006); 10.1063/1.2408650

[The influence of an extrinsic interfacial layer on the polarization of sputtered Ba Ti O 3 film](#)

Appl. Phys. Lett. **86**, 202905 (2005); 10.1063/1.1921358

[Frequency response and scaling of hysteresis for ferroelectric Pr\(Zr 0.52 Ti 0.48 \)O 3 thin films deposited by laser ablation](#)

J. Appl. Phys. **86**, 5198 (1999); 10.1063/1.371500

[Pyroelectric hysteresis loop at ferroelectric phase transition](#)

J. Appl. Phys. **85**, 4256 (1999); 10.1063/1.370339

MIT LINCOLN
LABORATORY
CAREERS

Discover the satisfaction of
innovation and service
to the nation

- Space Control
- Air & Missile Defense
- Communications Systems & Cyber Security
- Intelligence, Surveillance and Reconnaissance Systems
- Advanced Electronics
- Tactical Systems
- Homeland Protection
- Air Traffic Control

 **LINCOLN LABORATORY**
MASSACHUSETTS INSTITUTE OF TECHNOLOGY



Influence of interfacial dislocations on hysteresis loops of ferroelectric films

Y. L. Li,^{1,a)} S. Y. Hu,² S. Choudhury,¹ M. I. Baskes,³ A. Saxena,⁴ T. Lookman,⁴ Q. X. Jia,⁵ D. G. Schlom,¹ and L. Q. Chen¹

¹*Department of Materials Science and Engineering, Pennsylvania State University, University Park, Pennsylvania 16802, USA*

²*Engineering Mechanics and Structural Materials, Pacific Northwest National Laboratory, Richland, Washington 99354, USA*

³*Los Alamos National Laboratory, MST-8, MS G755, Los Alamos, New Mexico 87545, USA*

⁴*Los Alamos National Laboratory, T-11, MS B262, Los Alamos, New Mexico 87545, USA*

⁵*Los Alamos National Laboratory, MPA-STC, MS K763, Los Alamos, New Mexico 87545, USA*

(Received 29 May 2008; accepted 4 October 2008; published online 19 November 2008)

We investigated the influence of dislocations, located at the interface of a ferroelectric film and its underlying substrate, on the ferroelectric hysteresis loop including the remanent polarization and coercive field using phase-field simulations. We considered epitaxial ferroelectric BaTiO₃ films and found that the hysteresis loop is strongly dependent on the type and density of interfacial dislocations. The dislocations that stabilize multiple ferroelectric variants and domains reduce the coercive field, and consequently, the corresponding remanent polarization also decreases. © 2008 American Institute of Physics. [DOI: [10.1063/1.3021354](https://doi.org/10.1063/1.3021354)]

I. INTRODUCTION

An important characteristic of ferroelectrics is the hysteresis loop of polarization versus applied electric field, which describes the switching behavior of spontaneous polarization.¹ It directly affects the performance of nonvolatile memories² in various applications of ferroelectric thin films. The hysteresis loops are characterized by the remanent polarizations (the polarization after the applied electric field decreases to zero) and the coercive fields (the value of the electric field required to reduce polarization to zero) and are highly dependent on the ferroelectric structure in the film, the localized nucleation of domains with reversed polarization, and domain wall mobility.^{3–9} Defects such as dislocations, space charge, domain or/and grain boundaries, and porosity arising from film fabricating processes are invariably the nucleation sites of domains with reversed polarization during polarization switching.^{10–12}

In the course of film growth and ferroelectric transitions below the Curie temperature, the presence of dislocations at the interface between the film and substrate is usually unavoidable due to the lattice mismatch and different thermal expansions.^{13–19} Although it is known that dislocations alter the ferroelectric properties of the films, it is quite difficult in experiments to identify the role played by different types of dislocations with differing densities in determining ferroelectric properties. The objective of this work is therefore to examine the role of interfacial dislocations on the behavior of ferroelectric hysteresis loops using phase-field modeling, which has successfully predicted ferroelectric transition temperatures and domain structures in ferroelectric films and superlattices.^{20–22} It has also yielded insight into how the presence of interfacial dislocations locally modifies the ferroelectric transition temperature and leads to the preferen-

tial formation of ferroelectric domains around misfit dislocations.²³ Here we will show that the coercive field and remanent polarization are strongly dependent on the type and density of the interfacial dislocations. The dislocations that stabilize multiple ferroelectric variants and domains reduce the coercive field and remanent polarization. This has a direct bearing on the control and optimization of the switching behavior of ferroelectric films for applications.

Two types of dislocations, misfit dislocations and threading dislocations, are often observed in epitaxial ferroelectric thin films.^{14–19} The misfit dislocations lie in the interface to accommodate the lattice mismatch between the film and substrate. It is commonly accepted that threading dislocations are formed in the film by the glide of a dislocation half loop terminated at the surface, driven by the misfit stresses during growth.^{16,24} The final dislocation line consists of one misfit segment on the interface and two segments that thread from the interface to the surface. In this work, these two types of dislocations are taken into account in a cubic perovskite film heteroepitaxially grown on a substrate with a square or rectangular surface net. We assume that a periodic dislocation array is formed at the interface during film growth at high temperature or/and during the ferroelectric transition just below the Curie temperature. The Burgers vectors of dislocations are assumed to be along $\langle 100 \rangle$ and $\langle 1-10 \rangle$ of the pseudocubic crystallographic axes of the film, respectively. The dislocations remain stationary during polarization switching.

II. PHASE FIELD MODELING

In order to describe the ferroelectric domain structure in the film and its evolution under an applied external electric field, the spontaneous polarization $\mathbf{P}=(P_1, P_2, P_3)$ is chosen as the order parameter. The total free energy of the film is calculated by

^{a)}Electronic mail: yill@psu.edu.

$$F = \int_V (f_{\text{bulk}} + f_{\text{grad}} + f_{\text{elas}} + f_{\text{elec}}) dV, \quad (1)$$

where V is the volume of the film. In the equation, f_{bulk} is the bulk free energy density of the ferroelectric material and is expressed by the Landau polynomial expansion in terms of the polarization components

$$\begin{aligned} f_{\text{bulk}} = & \alpha_1(P_1^2 + P_2^2 + P_3^2) + \alpha_{11}(P_1^4 + P_2^4 + P_3^4) + \alpha_{12}(P_1^2 P_2^2 \\ & + P_2^2 P_3^2 + P_1^2 P_3^2) + \alpha_{111}(P_1^6 + P_2^6 + P_3^6) + \alpha_{112}[P_1^2(P_2^4 \\ & + P_3^4) + P_2^2(P_1^4 + P_3^4) + P_3^2(P_1^4 + P_2^4)] + \alpha_{123}P_1^2 P_2^2 P_3^2 \\ & + \alpha_{1111}(P_1^8 + P_2^8 + P_3^8) + \alpha_{1112}[P_1^6(P_2^2 + P_3^2) + P_2^6(P_1^2 \\ & + P_3^2) + P_3^6(P_1^2 + P_2^2)] + \alpha_{1122}(P_1^4 P_2^4 + P_2^4 P_3^4 + P_1^4 P_3^4) \\ & + \alpha_{1123}(P_1^4 P_2^2 P_3^2 + P_2^4 P_3^2 P_1^2 + P_3^4 P_1^2 P_2^2), \end{aligned} \quad (2)$$

where all of the coefficients are assumed to be temperature independent except α_1 . α_1 is linearly dependent on temperature and obeys the Curie–Weiss law. f_{grad} in Eq. (1) is the gradient energy density. It is only nonzero around domain walls and calculated through the gradients of the polarization field

$$f_{\text{grad}} = \frac{1}{2} G_{ijkl} P_{i,j} P_{k,l}, \quad (3)$$

where $P_{i,j} = \partial P_i / \partial x_j$, and G_{ijkl} are the gradient energy coefficients with the property of $G_{ijkl} = G_{klij}$. The summation convention for the repeated indices is employed and $i, j, k, l = 1, 2, 3$.

The elastic energy f_{elas} is generated from the phase transition and the substrate constraint and is expressed generally by

$$f_{\text{elas}} = \frac{1}{2} c_{ijkl} e_{ij} e_{kl} = \frac{1}{2} c_{ijkl} (\varepsilon_{ij} - \varepsilon_{ij}^0) (\varepsilon_{kl} - \varepsilon_{kl}^0), \quad (4)$$

where c_{ijkl} is the elastic stiffness tensor, $e_{ij} = \varepsilon_{ij} - \varepsilon_{ij}^0$ is the elastic strain, ε_{ij} is the total strain, and ε_{ij}^0 is the stress-free strain or eigenstrain. Both ε_{ij} and ε_{ij}^0 are defined using the pseudocubic phase as the reference. The eigenstrain connected with the ferroelectric transition is $\varepsilon_{ij}^{0,P} = Q_{ijkl} P_k P_l$, where Q_{ijkl} represents the electrostrictive coefficient.

Dislocations are viewed as one kind of lattice distortion. The eigenstrain tensor related to a dislocation loop s on a slip plane $\mathbf{n}^s = (n_1^s, n_2^s, n_3^s)$ with a Burgers vector $\mathbf{b}^s = (b_1^s, b_2^s, b_3^s)$ can be described as^{25–27}

$$\varepsilon_{ij}^{0,s}(\mathbf{x}) = \frac{1}{2d_0^s} (b_i^s n_j^s + b_j^s n_i^s) \delta(\mathbf{x} - \mathbf{x}_0^s), \quad (5)$$

where \mathbf{n}^s is the unit vector normal to the slip plane, d_0^s is the interplanar distance of the slip planes, and $\delta(\mathbf{x} - \mathbf{x}_0^s)$ is the Dirac delta function with \mathbf{x}_0^s being a point inside the dislocation loop on the slip plane. For a spatial distribution of many dislocation loops, the total eigenstrain $\varepsilon_{ij}^{0,\text{dis}}(\mathbf{x})$ can be obtained by adding the eigenstrain tensor of individual dislocation loops, i.e., $\varepsilon_{ij}^{0,\text{dis}}(\mathbf{x}) = \sum_{s=1}^S \varepsilon_{ij}^{0,s}(\mathbf{x})$. So the total eigenstrain in the considered film-substrate system is $\varepsilon_{ij}^0 = \varepsilon_{ij}^{0,P} + \varepsilon_{ij}^{0,\text{dis}}$. The strain ε_{ij} can be obtained using a combination of Khachaturyan's mesoscopic elasticity theory^{28,29} and the Stroh formalism of anisotropic elasticity.^{30,31} Details are given in Ref. 32.

The electrostatic energy density of a given polarization distribution is calculated by

$$f_{\text{elec}} = -\frac{1}{2} E_i (\omega_0 \kappa E_i + P_i), \quad (6)$$

where E_i is the electric field component. It is related to the electric displacement D_i through the usual relation $D_i = \omega_0 \kappa E_i + P_i$, in which $\omega_0 = 8.85 \times 10^{-12}$ F m⁻¹ is known as the dielectric permittivity of a vacuum, and κ is the relative dielectric permittivity of the bulk background.

Suppose there is no space charge inside the film, the electric displacement D_i satisfies the electrostatic equilibrium equation of $D_{i,i} = 0$ in the film. On the top and bottom surfaces of the film, $\varphi|_{x_3=0} = \varphi_1$, $\varphi|_{x_3=h_f} = \varphi_2$ if the electric potential ϕ is specified on both surfaces of the film, where h_f is the film thickness. ϕ is related to E_i through $E_i = -\varphi_{,i}$, where $\varphi_{,i} = \partial \varphi / \partial x_i$. Therefore, the electrostatic equilibrium equation is cast into $\omega_0 \kappa (\phi_{11} + \phi_{22} + \phi_{33}) = P_{1,1} + P_{2,2} + P_{3,3}$. We employ the same methodology to solve the electrostatic equilibrium equation as that used in solving the elastic equilibrium equations in Ref. 32. For simplicity, we do not consider the incomplete screening by the electrodes as discussed in Ref. 33. The effect of multidomain emphasized in Ref. 34 will be automatically taken into account since there is no restriction on the polarization distribution by the simulations.

The temporal evolution of the polarization \mathbf{P} and thus the domain structures are described by the time dependent Ginzburg–Landau equations

$$\frac{\partial P_i(\mathbf{x}, t)}{\partial t} = -L \frac{\delta F}{\delta P_i(\mathbf{x}, t)} \quad (i = 1, 2, 3), \quad (7)$$

where L is the kinetic coefficient correlated with the domain mobility and $\delta F / \delta P_i(\mathbf{x}, t)$ is the thermodynamic driving force for the spatial and temporal evolution of $P_i(\mathbf{x}, t)$.

III. P-E HYSTERESIS LOOPS

We employ the semi-implicit Fourier-spectral method³⁵ to solve the evolution equations in Eq. (7). A model size of $64\Delta x \times 64\Delta x \times 32\Delta x$ is used and periodic boundary conditions are applied along the in-plane x_1 and x_2 axes. Δx is the grid spacing. The thickness of the film is taken as $h_f = 12\Delta x$. The region of the substrate allowed to relax the inhomogeneous elastic deformation is assumed to be $h_s = 12\Delta x$. BaTiO₃ is taken as the model material.^{8,9,13,36–40} The corresponding Landau energy coefficients, elastic constants, and electrostrictive coefficients employed in the simulations are listed in Ref. 41, which were from Refs. 42–45. The film is clamped by its underlying substrate, i.e., the average in-plane strains of the film are assumed to be $\bar{\varepsilon}_{11} = \bar{\varepsilon}_{22} = \bar{\varepsilon}_{12} = 0$. The gradient energy is assumed to be isotropic and the sole independent nonzero coefficient is taken as $G_{1111} / G_0 = 0.6$, where G_0 is related to the magnitude of Δx through $\Delta x = \sqrt{G_0 / \alpha_0}$ and $\alpha_0 = |\alpha_1|_{T=25^\circ\text{C}}$. The time step for the evolution in Eq. (6) is $\Delta t / t_0 = 0.02$, where $t_0 = 1 / (\alpha_0 L)$. The simulations are done at room temperature and the relative dielectric permittivity is assumed to be $\kappa = 200$.

In order to simulate the hysteresis loop, an electric potential is applied to the top electrode of the film while the bottom electrode is grounded. The simulation starts from an

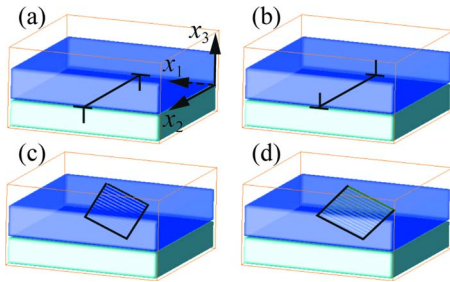


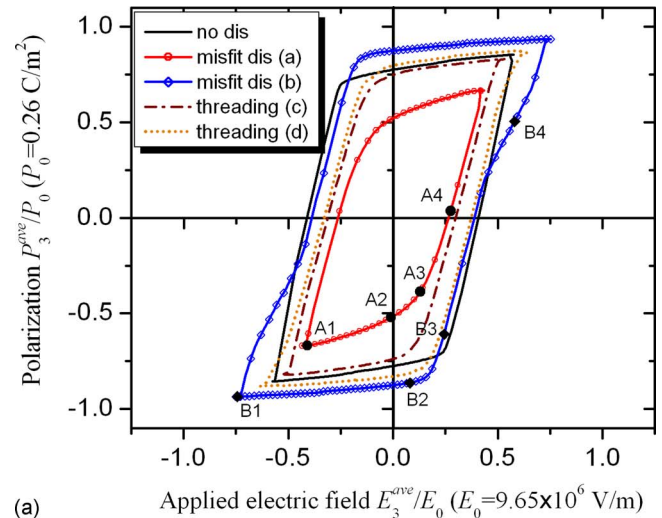
FIG. 1. (Color online) Schematic illustrations of simulated models: (a) misfit dislocation with $\mathbf{b}^s = [-100]$ and $\mathbf{n}^s = (100)$, (b) misfit dislocation with $\mathbf{b}^s = [100]$ and $\mathbf{n}^s = (100)$, (c) threading dislocation with $\mathbf{b}^s = [1-10]$ and $\mathbf{n}^s = (111)$, and (d) threading dislocation with $\mathbf{b}^s = [10-1]$ and $\mathbf{n}^s = (111)$.

initial paraelectric state with small random perturbations. Depolarizing fields along both the in-plane x_1 and x_2 directions are considered. At each increment of the electric potential ($0.08E_0\Delta x$), the domain structure from a previous simulation (after 1000 iterations) is used as the input. The hysteresis loop is obtained by plotting the normalized average polarization (P_3^{ave}/P_0) versus the normalized electric field (E_3^{ave}/E_0) along the x_3 direction, where the average is taken over the whole film, $E_0 = \alpha_0 P_0 = 9.65 \times 10^6 \text{ V m}^{-1}$ and $P_0 = |P|_{T=25^\circ\text{C}} = 0.26 \text{ C m}^{-2}$.

A. Effect of dislocation type

Figure 1 schematically shows the simulation cell and dislocation configurations considered in this work. Figure 1(a) shows an edge dislocation on the interface. The edge dislocation has an extra half atomic plane inserted in the substrate with a normal vector $\mathbf{n}^s = (100)$ and a Burgers vector $\mathbf{b}^s = [-100]$. Figure 1(b) exhibits another edge dislocation with a Burgers vector of $\mathbf{b}^s = [100]$ associated with a half atomic plane of $\mathbf{n}^s = (100)$ removed from the substrate. Figures 1(c) and 1(d) show the threading dislocations consisting of one misfit segment with length of $40\Delta x$ on the interface and two screw segments that thread from the interface to the surface. They are all on the slip plane of $\mathbf{n}^s = (111)$ but with different Burgers vector $\mathbf{b}^s = [1-10]$ (c) and $\mathbf{b}^s = [10-1]$ (d), respectively.

Taking into account each of the dislocations shown in Fig. 1, we obtained the polarization-electric field hysteresis loops. They are presented in Fig. 2(a). It clearly demonstrates that the presence of different types of dislocations affects the hysteresis loops, including the coercive electric field and remanent polarization. The hysteresis loop for the film containing dislocation (a) with $\mathbf{b}^s = [-100]$ and $\mathbf{n}^s = (100)$ has the smallest coercive field and remanent polarization. This is because the tensile stress in the film along the x_1 direction resulting from dislocation (a) promotes the formation of domains with polarizations lying in the film plane so that the remanent polarization along the out-of-plane direction decreases. On the other hand, the domain structure containing multiple variants provides more nucleation sites for new domains with opposite P_3 component, which prefer to nucleate at the domain junctions or interfaces of the different variants, thus reduces the resistance of switching and the coercive field. As misfit dislocation (b) with $\mathbf{b}^s = [100]$ and $\mathbf{n}^s = (100)$



(a) Applied electric field E_3^{ave}/E_0 ($E_0 = 9.65 \times 10^6 \text{ V/m}$)

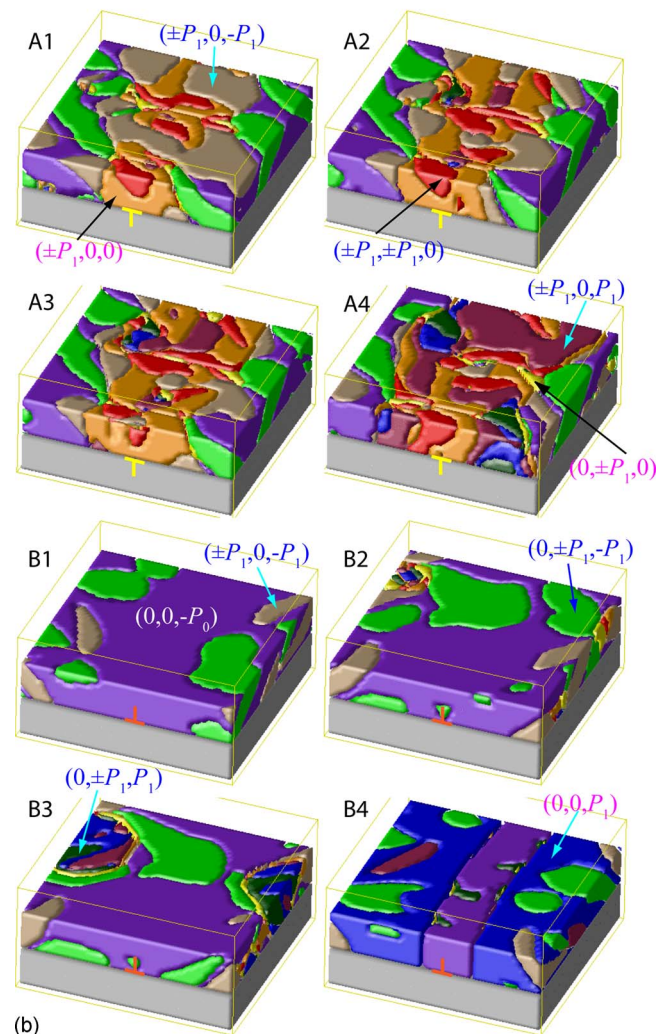


FIG. 2. (Color online) (a) Hysteresis loops for BaTiO₃ films with different types of interfacial dislocations. (b) Domain morphologies at the points shown in (a). Each color represents one type of domain. The corresponding polarization is indicated in the figures.

favors polarizations along the out-of-plane direction, the corresponding remanent polarization has a maximum. However, the corresponding coercive field does not increase compared to the case without any dislocation, which is very encouraging. We have noticed that there are bumps on the P - E hys-

teresis loop at $|E| > 0.4E_0$. It should be due to domain pinning at the dislocation line. But the pinning is not at the nucleation of the new domains with P_3 along the direction of the applied electric field. Instead, it is at the growth of these new domains.

For the film with a threading dislocation on the slip plane of $\mathbf{n}^s=(111)$ with Burgers vector $\mathbf{b}^s=[1-10]$ [labeled as (c) in Fig. 2(a)] or $\mathbf{b}^s=[10-1]$ [labeled as (d) in Fig. 2(a)], the corresponding hysteresis loop is between the films with the misfit dislocations (a) and (b), respectively. As we already knew from Fig. 1, the threading dislocation consists of one misfit segment on the interface and two screw segments that thread from the interface to the surface through the slip plane of $\mathbf{n}^s=(111)$. Simulations show that threading dislocations easily result in asymmetric coercive fields for the negative and positive applied voltages, as shown in Fig. 2(a).

Some typical domain structures during domain switching are displayed in Fig. 2(b), corresponding to the points shown in Fig. 2(a). Each color in the domain morphologies represents one type of domain. The corresponding polarization for each color is indicated in the figures. Due to the existence of dislocations and clamping from the substrate, orthorhombic phases are stabilized in the films besides the well known tetragonal phase. In the figures, the domains having positive or negative P_1 and/or P_2 are not distinguished since we are mainly concerned with the switching of P_3 . The domain morphologies clearly showed that the misfit dislocation (a) with $\mathbf{b}^s=[-100]$ and $\mathbf{n}^s=(100)$ promotes P_1 , so nearby the dislocation, the domains having the polarization of $(\pm P_0, 0, 0)$ or $(\pm P_0, 0, \pm P_0)$ dominate. On the other hand, the misfit dislocation (b) with $\mathbf{b}^s=[100]$ and $\mathbf{n}^s=(100)$ promotes P_3 but depresses P_1 , thus no domain of $(\pm P_0, 0, 0)$ or $(\pm P_0, 0, \pm P_0)$ appears near the dislocation. For a given misfit dislocation, whether the domains with positive P_3 or those with negative P_3 dominate the domain structure depends on the applied electric field. It can be seen from the domain morphologies that the volume fraction of the domains having polarization of $(0, 0, P_0)$, $(\pm P_0, 0, P_0)$, or $(0, \pm P_0, P_0)$ increases with increasing applied electric field.

B. Effect of dislocation density

In order to consider the effect of the dislocation density, we consider misfit dislocations of type (a) with $\mathbf{n}^s=(100)$ and $\mathbf{b}^s=[-100]$ and of type (b) with $\mathbf{n}^s=(100)$ and $\mathbf{b}^s=[100]$, which, respectively, correspond to the inner and outer boundaries of the hysteresis loops shown in Fig. 2(a). The results are presented in Fig. 3. The dislocations considered here are uniformly and periodically distributed. Since the size of the simulation cell is fixed, the spacing between the dislocations is $64\Delta x$ when there is only one dislocation, $32\Delta x$ when there are two dislocations, and $21\Delta x$ when there are three dislocations, respectively. In our simulations, Δx is about 2 nm, so the distance between dislocations is about 128, 64, and 42 nm, respectively, when there are one, two, and three dislocations considered. We see that the remanent polarization and coercive field decrease rapidly with increasing dislocation density of type (a) [see Fig. 3(a)]. In the case of $3 \times (a)$, the corresponding hysteresis loop becomes very narrow, similar

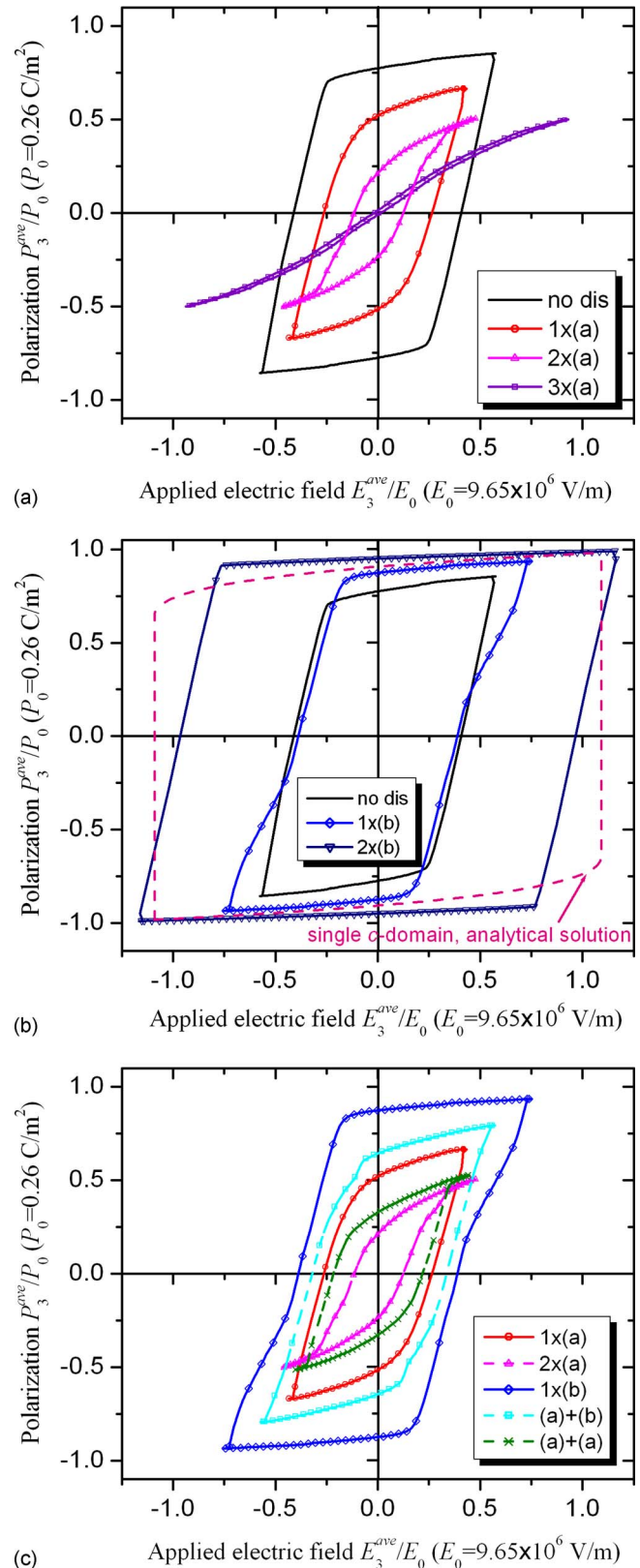


FIG. 3. (Color online) Hysteresis loops for BaTiO₃ films with different densities of type (a) and type (b) interfacial misfit dislocations. The notation of $2 \times (a)$ indicates that two dislocations of type (a) distribute uniformly along the x_1 -direction. The notation of $(a)+(b)$ indicates that one dislocation of type (a) is along the x_1 -direction and one dislocation of type (b) is along the x_2 -direction, respectively. The other notations have similar meanings.

to that of a dielectric. The experimentally observed narrow hysteresis loops might be due to the existence of interface

dislocations of type (a).⁹ It should be pointed out, however, that the disappearance of the hysteresis loop does not mean the disappearance of ferroelectricity in the film. It implies that the polarization prefers to orientate parallel to the film surface.³⁸ Actually dislocations of type (a) enhance the in-plane spontaneous polarization of the film. The remanent polarization almost being zero depicted in Fig. 3(a) is due to the fact that only the out-of-plane component contributes to the remanent polarization.

Figure 3(b) shows that the coercive field for the case of $2 \times (b)$ is more than twice of the case of $1 \times (b)$ with only a slight increase in the remanent polarization. The hysteresis loop for the case of $2 \times (b)$ is close to that from the analytical solution on the base of a single tetragonal *c*-domain. Domain visualizations illustrate that in such a case, the domain structure at the maximum electric field is a quasisingle tetragonal *c*-domain with slightly inhomogeneous distribution of P_3 near the film surfaces. Actually the existed dislocations in the case of $2 \times (b)$ produce more compressive strain ε_{11} than that in a single tetragonal *c*-domain, which increases domain pinning. However, the inhomogeneous distribution of P_3 still decreases the coercive field compared to the single domain case. As pointed above, the spacing between dislocations is about 64 nm in the case of $2 \times (b)$. The corresponding dislocation density is high in comparing with experimental observations.

As shown in Figs. 3(a) and 3(b), dislocation (a) reduces the coercive field and dislocation (b) enhances the remanent polarization. The combination of (a)+(b) is expected to give an optimal case, which have a smaller coercive field but a relatively larger remanent polarization. Figure 3(c) demonstrates it does. On the other hand, dislocations of (a)+(a) have less effect than that of $2 \times (a)$ for reducing remanent polarization and coercive field even if the density of the dislocations is the same at both cases. The notation of (a)+(a)/(b) indicates that there is a dislocation of type (a) along the x_1 -direction and a dislocation of type (a) or (b) along the x_2 -direction in the simulation cell.

IV. CONCLUSION

In summary, we have used a phase-field model for studying the effect of interfacial dislocations on the hysteresis loops of ferroelectric polarization versus applied electric field for BaTiO₃ thin films. We found that (1) increasing the density of interfacial misfit dislocations with $\mathbf{b}^s = [-100]$ and $\mathbf{n}^s = (100)$ narrows the hysteresis loop or decreases the coercive field, (2) threading dislocations cause an asymmetric coercive fields for the negative and positive applied voltages, and (3) an optimal combination of misfit dislocations with $\mathbf{b}^s = [-100]$ and $\mathbf{n}^s = (100)$ and misfit dislocations with $\mathbf{b}^s = [010]$ and $\mathbf{n}^s = (010)$ can produce a relatively smaller coercive field but larger remanent polarization. These may shed light on how to enhance or reduce coercive field and remanent polarization by deliberately introducing or avoiding interfacial dislocations in specific applications.

ACKNOWLEDGMENTS

This work was supported by the Laboratory-Directed Research and Development Program under DOE at Los Alamos National Laboratory, NSF under Grant Nos. DMR-0507146 and DMR-0820404, and the Department of Energy under Grant No. DE-FG02-07ER46417.

- ¹F. Jona and G. Shirane, *Ferroelectric Crystals* (Pergamon, Oxford, 1962).
- ²J. F. Scott and C. A. P. Dearaujo, *Science* **246**, 1400 (1989).
- ³C. M. Foster, G. R. Bai, R. Csencsits, J. Vetrone, R. Jammy, L. A. Wills, E. Carr, and J. Amano, *J. Appl. Phys.* **81**, 2349 (1997).
- ⁴M. B. Kelman, P. C. McIntyre, B. C. Hendrix, S. M. Bilodeau, and J. F. Roeder, *J. Appl. Phys.* **93**, 9231 (2003).
- ⁵K. S. Lee, Y. K. Kim, S. Baik, J. Kim, and I. S. Jung, *Appl. Phys. Lett.* **79**, 2444 (2001).
- ⁶T. Oikawa, M. Aratani, H. Funakubo, K. Saito, and M. Mizuhira, *J. Appl. Phys.* **95**, 3111 (2004).
- ⁷M. Klee, R. Eusemann, R. Waser, W. Brand, and H. Vanhal, *J. Appl. Phys.* **72**, 1566 (1992).
- ⁸H. B. Sharma and A. Mansingh, *J. Phys. D* **31**, 1527 (1998).
- ⁹R. Kullmer, *Appl. Phys. A: Mater. Sci. Process.* **65**, 273 (1997).
- ¹⁰K. Lee and S. Baik, *Annu. Rev. Mater. Res.* **36**, 81 (2006).
- ¹¹N. Setter, D. Damjanovic, L. Eng, G. Fox, S. Gevorgian, S. Hong, A. Kingon, H. Kohlstedt, N. Y. Park, G. B. Stephenson, I. Stolitchnov, A. K. Tagansteu, D. V. Taylor, T. Yamada, and S. Streiffer, *J. Appl. Phys.* **100**, 051606 (2006).
- ¹²V. Nagarajan, C. L. Jia, H. Kohlstedt, R. Waser, I. B. Misirlioglu, S. P. Alpay, and R. Ramesh, *Appl. Phys. Lett.* **86**, 192910 (2005).
- ¹³J. P. Gong, M. Kawasaki, K. Fujito, U. Tanaka, N. Ishizawa, M. Yoshimoto, H. Koinuma, M. Kumagai, K. Hirai, and K. Horiguchi, *Jpn. J. Appl. Phys., Part 2* **32**, L687 (1993).
- ¹⁴R. Beanland, D. J. Dunstan, and P. J. Goodhew, *Adv. Phys.* **45**, 87 (1996).
- ¹⁵H. P. Sun, W. Tian, X. Q. Pan, J. H. Haeni, and D. G. Schlom, *Appl. Phys. Lett.* **84**, 3298 (2004).
- ¹⁶I. B. Misirlioglu, A. L. Vasiliev, S. P. Alpay, M. Aindow, and R. Ramesh, *J. Mater. Sci.* **41**, 697 (2006).
- ¹⁷M. W. Chu, I. Szafraniak, R. Scholz, C. Harnagea, D. Hesse, M. Alexe, and U. Gosele, *Nature Mater.* **3**, 87 (2004).
- ¹⁸H. J. Gao, C. L. Chen, B. Rafferty, S. J. Pennycook, G. P. Luo, and C. W. Chu, *Appl. Phys. Lett.* **75**, 2542 (1999).
- ¹⁹I. Vrejoiu, G. Le Rhun, N. D. Zakharov, D. Hesse, L. Pintilie, and M. Alexe, *Philos. Mag.* **86**, 4477 (2006).
- ²⁰K. J. Choi, M. Bieganski, Y. L. Li, A. Sharan, J. Schubert, R. Uecker, P. Reiche, Y. B. Chen, X. Q. Pan, V. Gopalan, L. Q. Chen, D. G. Schlom, and C. B. Eom, *Science* **306**, 1005 (2004).
- ²¹D. A. Tenne, A. Bruchhausen, N. D. Lanzillotti-Kimura, A. Fainstein, R. S. Katiyar, A. Cantarero, A. Soukiasian, V. Vaithyanathan, J. H. Haeni, W. Tian, D. G. Schlom, K. J. Choi, D. M. Kim, C. B. Eom, H. P. Sun, X. Q. Pan, Y. L. Li, L. Q. Chen, Q. X. Jia, S. M. Nakhmanson, K. M. Rabe, and X. X. Xi, *Science* **313**, 1614 (2006).
- ²²Y. L. Li and L. Q. Chen, *Appl. Phys. Lett.* **88**, 072905 (2006).
- ²³S. Y. Hu, Y. L. Li, and L. Q. Chen, *J. Appl. Phys.* **94**, 2542 (2003).
- ²⁴J. W. Matthews, *Epitaxial Growth* (Academic, New York, 1975), Vol. B.
- ²⁵F. R. N. Nabarro, *Philos. Mag.* **42**, 1224 (1951).
- ²⁶S. Y. Hu and L. Q. Chen, *Acta Mater.* **52**, 3069 (2004).
- ²⁷Y. U. Wang, Y. M. Jin, A. M. Cuitino, and A. G. Khachatryan, *Acta Mater.* **49**, 1847 (2001).
- ²⁸A. G. Khachatryan and G. A. Shatalov, *Sov. Phys. JETP* **29**, 557 (1969).
- ²⁹A. G. Khachatryan, *Theory of Structural Transformation in Solids* (Wiley, New York, 1983).
- ³⁰A. N. Stroh, *J. Math. Phys.* **41**, 77 (1962).
- ³¹T. C. T. Ting, *Anisotropic Elasticity: Theory and Applications* (Oxford University Press, New York, 1996).
- ³²Y. L. Li, S. Y. Hu, Z. K. Liu, and L. Q. Chen, *Acta Mater.* **50**, 395 (2002).
- ³³D. J. Kim, J. Y. Jo, Y. S. Kim, Y. J. Chang, J. S. Lee, J. G. Yoon, T. K. Song, and T. W. Noh, *Phys. Rev. Lett.* **95**, 237602 (2005).
- ³⁴A. M. Bratkovsky and A. P. Levanyuk, *Appl. Phys. Lett.* **89**, 253108 (2006).
- ³⁵L. Q. Chen and J. Shen, *Comput. Phys. Commun.* **108**, 147 (1998).
- ³⁶H. Nakazawa, H. Yamane, and T. Hirai, *Jpn. J. Appl. Phys., Part 1* **30**, 2200 (1991).
- ³⁷K. Nashimoto, D. K. Fork, F. A. Ponce, and J. C. Tramontana, *Jpn. J.*

- [Appl. Phys., Part 1](#) **32**, 4099 (1993).
- ³⁸H. A. Lu, L. A. Wills, and B. W. Wessels, [Appl. Phys. Lett.](#) **64**, 2973 (1994).
- ³⁹S. Tsunekawa, T. Fukuda, T. Ozaki, Y. Yoneda, and H. Terauchi, [Appl. Phys. Lett.](#) **71**, 1486 (1997).
- ⁴⁰V. Srikant, E. J. Tarsa, D. R. Clarke, and J. S. Speck, [J. Appl. Phys.](#) **77**, 1517 (1995).
- ⁴¹ $\alpha_1=4.124(T-115)\times 10^5$ $\alpha_{11}=-2.097\times 10^8$, $\alpha_{12}=7.974\times 10^8$, α_{111}
 $=1.294\times 10^9$, $\alpha_{112}=-1.950\times 10^9$, $\alpha_{123}=-2.500\times 10^9$, $\alpha_{1111}=3.863$
 $\times 10^{10}$, $\alpha_{1112}=2.529\times 10^{10}$, $\alpha_{1122}=1.637\times 10^{10}$, $\alpha_{1123}=1.367\times 10^{10}$, c_{11}
 $=1.78\times 10^{11}$, $c_{12}=0.964\times 10^{11}$, $c_{44}=1.22\times 10^{11}$, $Q_{11}=0.10$, $Q_{12}=-0.034$,
 $Q_{44}=0.029$ (in *Système International* units and T in °C).
- ⁴²Y. L. Li, L. E. Cross, and L. Q. Chen, [J. Appl. Phys.](#) **98**, 064101 (2005).
- ⁴³A. F. Devonshire, *Philos. Mag.* **42**, 1065 (1951).
- ⁴⁴D. Berlincourt and H. Jaffe, [Phys. Rev.](#) **111**, 143 (1958).
- ⁴⁵T. Yamada, [J. Appl. Phys.](#) **43**, 328 (1972).